

Interlayer and Intralayer Scale Aggregation for Scale-invariant Crowd Counting

Mingjie Wang^{1,2}, Hao Cai^{1,2}, Jun Zhou³, Minglun Gong²

¹ Memorial University of Newfoundland, NL, Canada

² University of Guelph, ON, Canada

³ Dalian Maritime University, Dalian, China

Abstract. Crowd counting is an important vision task, which faces challenges on continuous scale variation within a given scene and huge density shift both within and across images. These challenges are typically addressed using multi-column structures in existing methods. However, such an approach does not provide consistent improvement and transferability due to limited ability in capturing multi-scale features, sensitiveness to large density shift, and difficulty in training multi-branch models. To overcome these limitations, a Single-column Scale-invariant Network (ScSiNet) is presented in this paper, which extracts sophisticated scale-invariant features via the combination of interlayer multi-scale integration and a novel intralayer scale-invariant transformation (SiT). Furthermore, in order to enlarge the diversity of densities, a randomly integrated loss is presented for training our single-branch method. Extensive experiments on public datasets demonstrate that the proposed method consistently outperforms state-of-the-art approaches in counting accuracy and achieves remarkable transferability and scale-invariant property.

1 Introduction

Research in crowd counting has gained popularity in recent years due to its important real-world applications, such as video surveillance, traffic control, public security, and scene understanding [13,32,53,52,16]. With the unprecedented success of Convolutional Neural Networks (CNNs) in computer vision tasks, a series of CNN-based crowd counting algorithms have been developed in the past 6 years [18,22,55,36,42,28,34,20,23,27,25,43]. While these works have shown to be effective, accurate counting under challenging scenarios (e.g. severe occlusions, perspective effects, background clutter, scale variation, and density shift [48]) is still not yet achieved.

Previous studies have shown that scale variation in image to some extent limits the performance of designed models in vision tasks like object detection [24,1,31] and semantic segmentation [56,5,35]. This issue is even more pronounced in the field of crowd counting as the scale in those crowd images tends to vary continuously and dramatically. Fig. 1(a) shows examples of scale variation within a single image and density shift across crowded scenes.

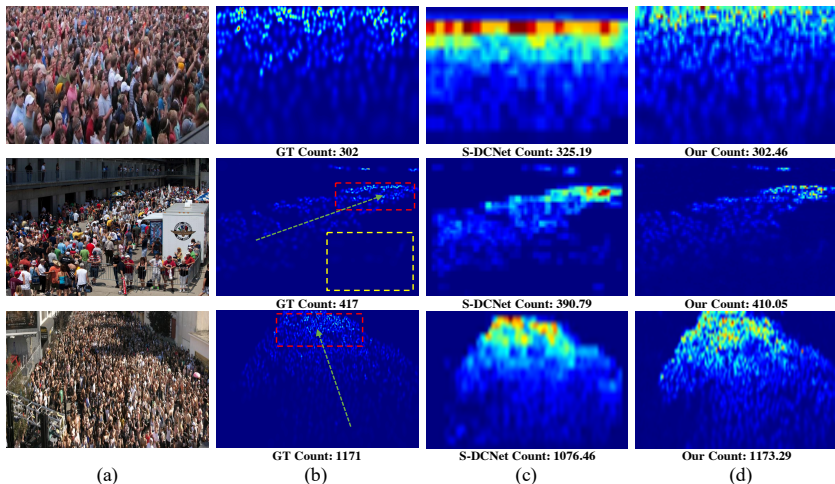


Fig. 1. Samples (a) taken from the ShanghaiTech Part_A dataset [55] demonstrate the challenges of continuous scale changes within a single image and high density shifts both within and across images. Green arrows in the ground truth (GT) density maps (b) show the directions of scale changes, whereas red and yellow rectangular boxes highlight high and low density areas, respectively. Compared to S-DCNet [47] (c), our method (d) handles these challenges much more effectively.

Considerable efforts have been made to deal with this issue by either utilizing multi-column CNNs [55,25,36] or a stack of multi-branch units [2] to extract features at multiple scales, or using skip connections to fuse feature maps from different layers by leveraging the fact that deeper layers produce higher-level information with larger reception fields [43,38,27,20] whereas shallower layers encode low-level spatial information for accurate localization. Nevertheless, these efforts largely lie on layer-wise multi-scale feature extraction in a coarse-grained fashion which takes the whole layer as input, resulting in insufficient diversity of scales. This inevitably affects the robustness and performance of their models. For instance, the S-DCNet [47], which has the lowest Mean Absolute Error (MAE) to date, does not generate accurate counts; see Fig. 1(c).

Recent work [45] has suggested that different channels of visual features are not entirely independent and they somewhat resemble traditional features like SIFT [29] and HOG [8], where each group of channels is constructed by some type of histogram. Motivated by this observation, we here propose to integrate both interlayer and intralayer scale fusion for scale-invariant crowd counting. To achieve intralayer scale fusion, different groups of feature channels are used to encode different regions of an image with varying receptive fields, allowing fine-grained multi-scale features to be captured. Combining this novel intralayer scale aggregation with the conventional interlayer multi-scale feature extraction allows the presented method to learn more sophisticated and diverse scale information, leading to more accurate performance; see Fig. 1(d).

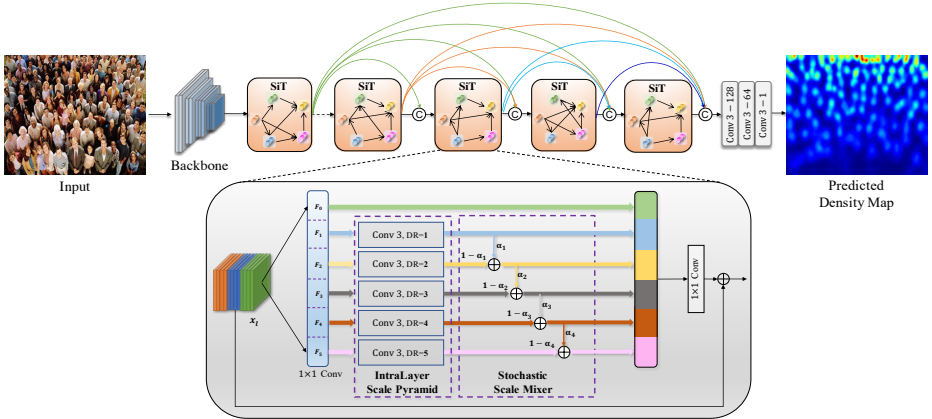


Fig. 2. Pipeline of the proposed ScSiNet for crowd counting. The backbone subnetwork is formed by the first ten layers of a pre-trained VGG-16 [41] to produce general features. The SiTs are combined by interlayer dense connections [17] and each SiT is comprised of an intralayer scale pyramid and a stochastic scale mixer. Specifically, the input of SiT is first processed by an 1×1 layer and then divided into $G = 6$ groups, denoted as F_0, \dots, F_5 . The scale pyramid performs dilated convolutions for groups F_1, \dots, F_5 with dilation rates (DR) ranging from 1 to 5. This is followed by the scale mixer, which is designed to blend the multi-scale features in a stochastic fashion. $\alpha_1, \alpha_2, \alpha_3, \alpha_4$ are random variables following the uniform distribution between 0 and 1.

Specifically, this paper presents a novel Single-column Scale-invariant Network (ScSiNet) architecture for crowd counting. As shown in Fig. 2, the proposed ScSiNet consists of a VGG-based backbone subnetwork, six scale-invariant transformation (SiT) layers with dense connections [17] in between, and output layers. The pattern of dense connections is leveraged to perform interlayer fusion of multi-level features through forwarding detailed features from shallower layers to all subsequent high-level layers. The SiT conducts fine-grained intralayer scale fusion and is the key component in our ScSiNet. Experimental results in Sec. 4 indicate that this novel SiT contributes to the robustness and stabilization of our model.

Furthermore, to overcome the grand effects of large density shifts and small training samples in crowd counting datasets like UCF_CC_50 [18], we introduce a simple yet effective objective function, which we call *randomly integrated loss*. Specifically, during each iteration, a batch of training sample patches with consistent resolution are randomly cropped and then processed separately by the model; see Sec. 3.3. Finally, an *integrated loss* is computed to optimize the network. In this way, the limited training sets can be better made use of and thus provides our model with resistance to overfitting. Moreover, the stochastic batch of patches with varying densities and integrated loss mitigate the density fluctu-

ations, thereby enabling our model to be robust to huge density shifts without using any multi-column structure.

The effectiveness of the proposed model is evaluated and compared against existing state-of-the-art methods on three widely-used datasets: ShanghaiTech [55], UCF-QNRF [19] and UCF_CC_50 [18]. Our contributions are summarized as follows:

- A novel intralayer scale-invariant transformation (SiT) module is designed, which effectively solves the problem of continuous scale variation in congested scenes and avoids potential overfitting.
- A randomly integrated loss is proposed, which significantly mitigates the effects of huge density shift in crowd datasets.
- The proposed ScSiNet outperforms the state-of-the-art methods and exhibits superior transferability and scale-invariance property, which are highly desired in real-world applications.

2 Related Work

Numerous algorithms are proposed in the past decade for counting objects in congested scenes. Traditional methods [12,10,44] primarily focus on counting-by-detection that explicitly detects individual objects being counted. Since the performance of detection is often affected by occlusion and background clutter, which in turn limits the accuracy of these counting-by-detection approaches. Later, the regression-based counting methods [4,3,21] improve the counting accuracy through learning a mapping between image features and total count/density map.

More recently, CNN-based crowd counting methods [18,22,55,36,42,28,34,20,23,27,25], have achieved dramatic improvements via the efforts in designing various creative architectures to handle the issues of scale and density variations. Notable works include MCNN [55], Switching-CNN [36], HydraCNN [32], AMDCN [9] and DSSINet [25]. These models aim at learning multi-branch regressors to extract and fuse multi-scale features, which improves the robustness with respect to scale variation. Meanwhile, a number of methods focus on other build techniques such as: *i*) bottom-top and top-bottom fusion of features from different layers [43]; *ii*) pursuing structural consistency in predicted density maps using auxiliary loss functions, such as composition loss [19], adversarial loss [37], SSIM [2,25], and Bayesian Loss [30]; *iii*) the use of dilation and deformable convolutions to enlarge the receptive fields [23,9,14,26]; *iv*) leveraging unlabeled data via a self-learning strategy [28] and negative correlation-based learning [40]; and *v*) utilizing attention mechanisms to adaptively aggregate multi-scale features [27,2,43,50]. More recently, efforts have been devoted to refining the sub-regions of predicted density maps. For instance, Cheng *et al.* [6] propose a new Maximum Excess over Pixels (MEP) loss to learn the spatial awareness, whereas Xu *et al.* [48] adopt multipolar center loss to bring the selected regions to multiple similar scale levels. Zhang *et al.* [50] and Liu *et al.* [25] propose to utilize conditional random fields to fuse complementary features.

Although the aforementioned CNN-based methods have made excellent progress in tackling scale variation, they all concentrate on layer-wise transformations, postprocessing, or ad-hoc loss terms, resulting in merely coarse-grained scale information. In comparison, we propose to perform intralayer, fine-grained scale fusion through assigning different groups of feature channels with receptive fields of different sizes. Integrating both interlayer and intralayer scale aggregation enhances our model with the capability of encoding multi-scale information from subregions of feature maps. Additionally, current crowd counting algorithms usually suffer from severe overfitting due to over-complex fusions or multi-branch structures, leading to poor generalization capability. To this end, Liu *et al.* [28] introduce a self-learning strategy leveraging abundant unlabeled images to alleviate overfitting, whereas Shi *et al.* [40] build decorrelated regressors to produce generalizable features. Both approaches are shown to be effective, but the performance gain is limited. Inspired by regularization techniques applied in the task of image classification, such as mixup [51] and shake-shake regularization [11], we design a novel scale mixer to fuse fine-grained multi-scale features via progressively stochastic convex combinations, which regularizes the scale dimension and further boosts the transferability and scale invariance of our model.

3 Proposed Method

3.1 Interlayer Dense Connections

It is well known that different layers in deep neural networks correspond to different receptive fields and semantic levels. Generally, representations from shallow layers have smaller semantic levels, and the encoded low-level spatial details can be used to obtain better localization [43]. Meanwhile, high-level features extracted by deeper layers have larger scales, which facilitate the retrieval of contextual information. Intuitively, in order to exploit the merits of multi-level features for crowd counting, it is important to integrate features at different semantic levels/scales. As shown in Fig. 2 (top), we fuse layer-based multi-scale information through dense connections [17]. Specifically, for the l^{th} transformation, the input x_l at multiple layer-based scales can be formulated as $x_l = [y_0, y_1, \dots, y_{l-1}]$, where $[y_0, y_1, \dots, y_{l-1}]$ denotes the concatenation of multi-scale features from preceding layer $0, 1, \dots, l-1$.

As mentioned in Sec. 1, current CNN-based models of crowd counting rely heavily on *interlayer* multi-scale feature extraction to deal with the large scale variation, most of which utilizing multi-column CNNs or a stack of multi-branch units. The reuse of multi-scale features through dense connections enables the proposed network achieve comparable performance with a single-column architecture, which simplifies training and prevents overfitting. In addition, we also exploit *intralayer* multi-scale fusion to seek more diverse representation of scales at different granular levels, as discussed in the subsection below.

3.2 Intralayer Scale-invariant Transformation

Recent research [45] has demonstrated that feature vectors in deep CNNs are not unstructured vectors and hence it is reasonable to group channels and expect different groups to capture different visual cues, such as shapes, frequency, and textures. Successful applications of group-based convolutions have been found in the task of image classification [46,7,54]. Motivated by this, we believe that features in a given layer could be grouped in terms of image sub-regions with different scales. To this end, we design a novel intralayer scale-invariant transformation (SiT), which involves an intralayer scale pyramid and a stochastic scale mixer as shown in Fig. 2 (bottom). The scale pyramid has the benefit of guiding the network to learn multi-scale representations corresponding to independent sub-regions without increasing computational overhead. Given that traditional aggregation methods such as weighted summation or concatenation have limited abilities to approximate continuous scales and are prone to overfitting, the scale mixer is proposed to shuffle and regularize fine-grained multi-scale features through a progressively stochastic manner. The scale mixer enables the network with two-fold advantages: *i*) decorrelating the groups of scale pyramid to regularize the features at different scales; *ii*) reducing sensitivity to scale changes to some extent.

Intralayer Scale Pyramid Instead of capturing features using groups of standard 3×3 filters in other group-based models [46,7,54], we split a feature vector into G groups, where each group is empirically set to contain 64 channels [15]. Due to dense connections, the number of channels in the input x_l varies at different layer l . To convert different numbers of input channels to G groups of 64 channels, a 1×1 convolution layer is used. The output of the 1×1 convolution layer is denoted as $[F_0, F_1, F_2, \dots, F_{G-1}]$, where each F_i has 64 channels.

To guide different groups to capture varied scales, dilated convolutions with different dilation rates are used to build a scale pyramid. Dilated convolution has the advantage of enlarging receptive field sizes without increasing the number of parameters [23]. Specifically, here F_0 is fed directly to the output (without passing through convolutions) as it aims to preserve the high-frequency information. The remaining $G - 1$ groups go through dilated convolutions with dilation rates from 1 to $G - 1$, respectively, to capture features at corresponding scales. The obtained intralayer scale pyramid can be written as $[F_0, D_1(W_1, F_1), D_2(W_2, F_2), \dots, D_{G-1}(W_{G-1}, F_{G-1})]$, where $[,]$ denotes the concatenation of groups with different receptive fields and W_i represents the trainable parameters of dilation convolutions D_i with dilation rate i , $i \in [1, 2, \dots, G - 1]$. Examples can be found in Fig. 2 (bottom), where it is divided into 6 groups and delivers 1×1 (F_0), 3×3 (D_1), ... , 11×11 (D_5) receptive fields respectively.

Stochastic Scale Mixer In the scale pyramid, each convolution only operates on the corresponding group of channels, which brings several side effects: *i*) The output from a certain group only relates to the input within the group [54] and

this blocks cross-group information communication; *ii*) The scale variation in crowd image is usually continuous and scale change boundaries are often fuzzy, whereas the pyramid can only generate strict boundaries of scales which could result in oversensitivity of the network.

To tackle these problems, a novel scale mixer is designed to progressively regularize and blend the multi-scale representations through a stochastic tree structure. For simplicity, we denote the outputs of scale pyramid and scale mixer as $[d_0, d_1, d_2, \dots, d_{G-1}]$, $[\hat{d}_0, \hat{d}_1, \hat{d}_2, \dots, \hat{d}_{G-1}]$, respectively. The procedure of scale mixer can be represented as a recursive function:

$$\begin{cases} \hat{d}_i = d_i, i = 0, 1 \\ \hat{d}_i = \alpha_{i-1} \times \hat{d}_{i-1} + (1 - \alpha_{i-1}) \times d_i, i = 2, \dots, G - 1, \end{cases} \quad (1)$$

where α_i are random variables following the uniform distribution between 0 and 1. Before each iteration in training, all variables are overwritten with new random values, while they are set to expected value of 0.5 at the test time. Taking $G = 6$ as an example, we deduce \hat{d}_5 as follows:

$$\begin{aligned} \hat{d}_5 = & \alpha_4 \hat{d}_4 + (1 - \alpha_4) d_5 = \alpha_4 [\alpha_3 \hat{d}_3 + (1 - \alpha_3) d_4] + (1 - \alpha_4) d_5 = \alpha_1 \alpha_2 \alpha_3 \alpha_4 d_1 \\ & + (1 - \alpha_1) \alpha_2 \alpha_3 \alpha_4 d_2 + (1 - \alpha_2) \alpha_3 \alpha_4 d_3 + (1 - \alpha_3) \alpha_4 d_4 + (1 - \alpha_4) d_5. \end{aligned} \quad (2)$$

Note that the mixer complements cross-scale features through a set of random variables, thus aiding in approximating the continuous scale change in crowd images and blur scale change boundaries. Moreover, the stochastic scale mixer is differentiable, which means it can be embedded into network for end-to-end training. Depending on the random variables, the scale mixer can smoothly vary its behaviour among multiple scales, thus helping produce more sophisticated and diverse scale information. Finally, feature maps transformed by the scale mixer are concatenated to be passed through an 1×1 convolutional layer to reduce the width of filters to 256 and assemble information together. To make our structure easier to be optimized, the paradigm of residual learning [15] is incorporated into our proposed SiT.

3.3 Randomly Integrated Loss

The current network training strategies for CNN-based counting models are mainly categorized into two classes: *i*) Original images or $1/4$ resolution patches are forwarded through the model one by one (batch size is 1) to optimize the network, where the training is dramatically affected by the number of samples and density shifts across the datasets; *ii*) A batch of patches randomly cropped in an off-line fashion are fed into the network and an average value of losses is obtained as the supervision. For instance, given the batch size N , the traditional loss [27,23,55] is computed as follows:

$$L = \frac{1}{2N} \sum_{i=1}^N \|Y_i - GT_i\|_2^2 = \sum_{i=1}^N \left\| \frac{1}{\sqrt{2N}} Y_i - \frac{1}{\sqrt{2N}} GT_i \right\|_2^2, \quad (3)$$

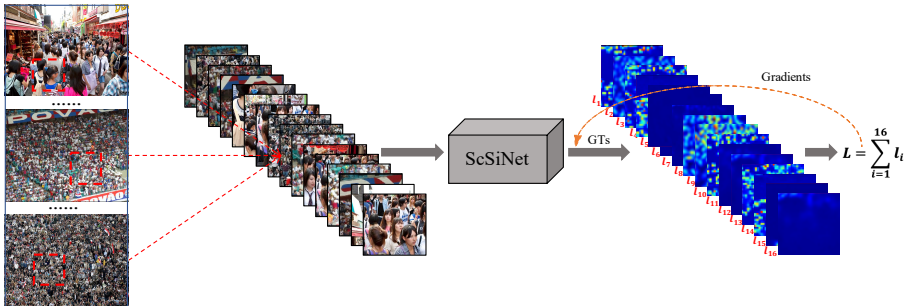


Fig. 3. Schema of randomly integrated loss with patch number $N = 16$. During each iteration, N patches randomly cropped from various original images are fed into our ScSiNet and finally an integrated loss is computed as the supervision.

where Y_i is the predicted density map for i^{th} image and GT_i means corresponding ground truth.

As it can be seen in Eq. 3, both Y_i and GT_i are divided by $\sqrt{2N}$ and their densities follow normal distribution $\mathcal{N}(0, \sigma^2)$ with variance σ indicating the range of densities in crowd datasets. As a result, this loss function inevitably changes the initial distributions and reduces the density diversity especially when the patch size is small or the batch size N is large. In this case, inappropriate cropping size and batch size easily lead to the difficulty of convergence or trapping in local optimal solutions. Although several attempts [30,48,47,27,19,25] have been made to overcome this issue by setting different sizes for each dataset or ad-hoc loss terms to remedy the the degradation of density diversity, these approaches often cause inconsistent improvements and degraded transferability across the datasets.

In this work, we propose a simple yet effective randomly integrated loss to better address the grand effects of large density shifts and limited training samples at widely-spread resolutions in crowd datasets. That is, during each iteration, we randomly crop patches online from original images with a constant resolution for all datasets and form the input with the batch size of N ; see Fig. 3. Instead of using an average value of losses as in Eq. 3, we obtain the batch loss by summing all sub-losses l_1, l_2, \dots, l_N , and the objective function is defined as:

$$L = l_1 + l_2 + \dots + l_N = \sum_{i=1}^N \|Y_i(x_i; W) - GT_i\|_2^2, \quad (4)$$

where W denotes the trainable parameters of the network, $Y_i(x_i; W)$ means the corresponding estimated density map patch and GT_i is the ground truth of x_i .

By feeding in randomly cropped patches, it allows our single-column model to possess the merits of “divide-and-conquer” without resorting to the extremely complicated patch-based subnetworks used by recent approaches [47,48]. Additionally, the limited training samples can be fully utilized, while the density range

is further enlarged and closely continuous, thereby enabling our single-column network to be easily trained and robust to huge density shifts.

4 Experimental Results

The following three widely used datasets are employed to evaluate the performance of our proposed method:

ShanghaiTech. The ShanghaiTech dataset contains 1,198 crowd images with a total of 330,165 annotated people and is divided into two parts. **Part_A** consists of 482 scenes with 300 images for training and the rest for testing. **Part_B** includes 716 images where 400 images are for training.

UCF-QNRF. This is the latest large-scale crowd dataset, containing 1,535 high resolution images with annotated people ranging from 49 to 12,865, thus making this dataset feature huge density variance. The training and testing sets consist of 1,201 and 334 images, respectively.

UCF_CC_50. The UCF_CC_50 dataset includes 50 annotated crowd images with crowd counts ranging from 94 to 4,543. This is a more challenging dataset due to the extremely limited number of samples. Following the standard protocol [18], we use 5-fold cross-validation to evaluate the performance of our proposed model on this dataset.

4.1 Implementation Details

Following the previous work [23], we use geometry-adaptive kernels with $\beta = 0.3$ and $k = 3$ to blur the annotated images for ShanghaiTech Part_A, whereas for Part_B, UCF-QNRF, and UCF_CC_50, we blur all head annotations using fixed Gaussian kernels with $\sigma = 15$ to generate ground-truth density maps. Our single-column structure is trained in an end-to-end fashion. We use Adam optimizer with a learning rate of 0.0001 to minimize the loss of Eq.4. At each training iteration, 16 image patches with a size of 176×176 are randomly cropped from original images. The first ten layers of the pre-trained VGG-16 are deployed to initialize the corresponding layers and the rest trainable weights are initialized by a normal distribution with zero mean and standard deviation of 0.01. We also add random horizontal flip for data augmentation following [43]. The proposed method is implemented with Pytorch [33]. Following previous work in this area [25], Mean absolute error (MAE) and mean square error (MSE) are also used as metrics to evaluate our model.

4.2 Comparison with the State-of-the-Arts

Table 1 compares the proposed ScSiNet with several state-of-the-art methods across three crowd counting datasets. The results show that our ScSiNet achieves the best MAE performance on ShanghaiTech Part_A, UCF-QNRF, and UCF_CC_50 datasets, even though its performance on Part_B is slightly lower than SPANet + SANet [6] and S-DCNet [47]. It is also worth noting that both UCF-QNRF

Table 1. Comparison with state-of-the-art methods on ShanghaiTech (Part_A and Part_B), UCF-QNRF and UCF_CC_50 datasets. Best results are shown in boldface.

Methods	Part_A		Part_B		UCF-QNRF		UCF_CC_50	
	MAE	MSE	MAE	MSE	MAE	MSE	MAE	MSE
TEDNet [20]	64.2	109.1	8.2	12.8	113	188	249.4	354.5
ADCrowdNet [26]	63.2	98.9	7.6	13.9	-	-	257.1	363.5
PACNN + CSRNet [38]	62.4	102.0	7.6	11.8	-	-	241.7	320.7
CAN [27]	62.3	100.0	7.8	12.2	107	183	212.2	243.7
CFF [39]	65.2	109.4	7.2	12.2	-	-	-	-
SPN+L2SM [48]	64.2	98.4	7.2	11.1	104.7	173.6	188.4	315.3
MBTTBF-SCFB [43]	60.2	94.1	8.0	15.5	97.5	165.2	233.1	300.9
PGCNet [49]	57.0	86.0	8.8	13.7	-	-	244.6	361.2
BL [30]	64.5	104.0	7.9	13.3	92.9	163.0	237.7	320.8
DSSINet [25]	60.63	96.04	6.85	10.34	99.1	159.2	216.9	302.4
SPANet+SANet [6]	59.4	92.5	6.5	9.9	-	-	232.6	311.7
S-DCNet [47]	58.3	95.0	6.7	10.	104.4	176.1	204.2	301.3
ScSiNet (proposed)	55.77	90.23	6.79	10.95	89.69	178.46	154.87	199.42

and UCF_CC_50 are more challenging than ShanghaiTech, as UCF-QNRF has wider density distributions and larger image resolutions whereas UCF_CC_50 has the highest density images and extremely small training set. On UCF-QNRF, ScSiNet produces a significant improvement of 3.21↓ in MAE compared with the existing best approach (BL [30]). On UCF_CC_50, ScSiNet lowers the MAE from 188.4 produced by SPN+L2SM [48] to 154.87 (17.8% ↓), and MSE from 243.7 of CAN [27] to 199.42 (18.2% ↓).

Qualitative comparisons with S-DCNet [47] for three samples with different densities from the ShanghaiTech Part_A are presented in Fig. 1. As it can be seen that the presented ScSiNet estimates more accurate count and meanwhile generates higher-quality predicted density maps (Fig. 1(d)) with less noise than the current state-of-the-art S-DCNet [47] (Fig. 1(c)). Samples of the test cases from ShanghaiTech Part_B, UCF-QNRF, and UCF_CC_50 are demonstrated in Fig. 4. The computational time are also measured by calculating the average inference time on the test set of Part_A. Run on a single Titan Xp GPU, the average overhead of ScSiNet is about 0.072s per image, which is 64% faster than that of S-DCNet [47] at 0.20s per image.

4.3 Scale-invariant Tests

Robustness to Resolution Changes. Most of the crowd counting models are trained and tested on high-resolution images. This leads to high memory or computational costs and limits the generalization on devices with lower computational capacity, such as smart security cameras. Reducing the resolution of testing images changes scale distributions and hence causes performance drop for non-scale-invariant methods.

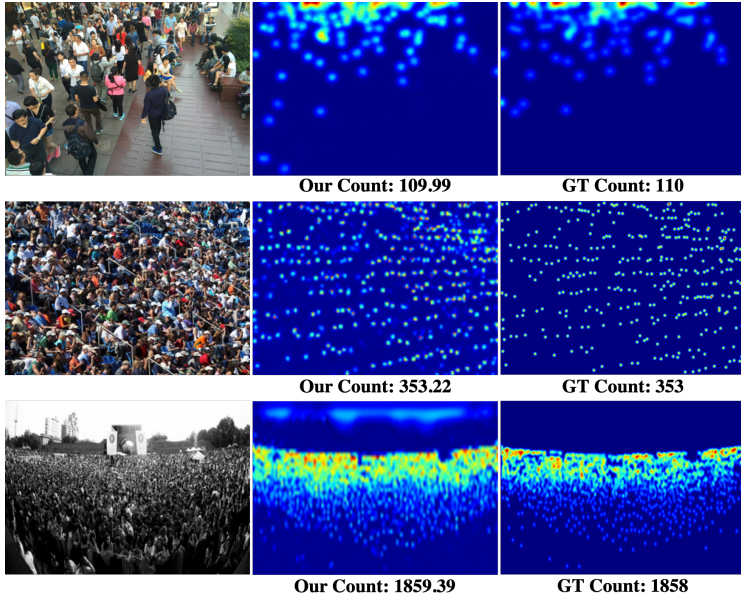


Fig. 4. Visualizations of prediction examples on ShanghaiTech Part_B (top), UCF-QNRF (middle), and UCF_CC_50 (bottom).

To test how well the proposed ScSiNet can handle resolution drops, we down-sample the test images from ShanghaiTech Part_A by various ratios, ranging from 100% (unchanged) to 16% (40% downsample in each dimension). The performances of ScSiNet and S-DCNet [47] on different resolution test images are plotted in Fig. 5. As expected, the MAE increases for both algorithms as image resolution drops. However, the increase for ScSiNet (Params. 14.1M) has a much slower rate than that of S-DCNet (Params. 28.24M). This indicates that ScSiNet can learn more scale-invariant features with less computational costs. In addition, when ScSiNet is fed with images downsampled by 81%, it achieves competitive MAE of 59.13, lower than those of MBTTBF-SCFB (60.2) [43], DSSINet (60.63) [25], and SPANet+SANet (59.4) [6] achieved on full-resolution images. Even using the images downsampled by 64%, ScSiNet still outperforms BL [30] (64.5), MPCL [48] (64.2), and Focus for free [39] (65.2).

Cross-dataset Transferability. To illustrate the transferability of our proposed ScSiNet, we conduct cross-data experiments, where the model is trained on one specific dataset and validated on other datasets without any retraining or fine-tuning. As can be seen from Table 2, our method consistently outperforms D-ConvNet [40] and SPN+L2SM [48] by a remarkable margin. Note that the ScSiNet model trained on UCF-QNRF even outperforms some methods on ShanghaiTech Part_A like ic-CNN [34] (MAE 69.8 and MSE 117.3) and L2R [28] (MAE 73.6 and MSE 112.0) that are trained on the same dataset. The superior trans-

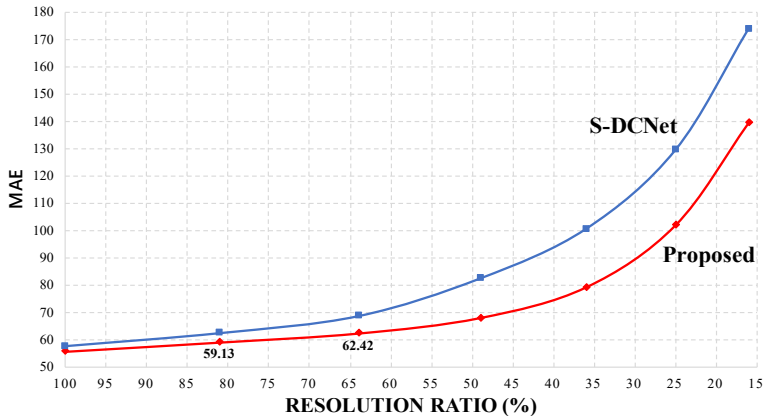


Fig. 5. Performance evaluation for ScSiNet and S-DCNet [47] on the original ShanghaiTech Part_A dataset (100%) and its downsampled versions. As image resolution reduces, the performance gain of ScSiNet over S-DCNet becomes more prominent.

Table 2. Cross-dataset evaluation for transferability comparison among different methods on ShanghaiTech A&B and UCF-QNRF (Q) datasets.

Methods	A→B		B→A		A→Q		Q→A	
	MAE	MSE	MAE	MSE	MAE	MSE	MAE	MSE
D-ConvNet [40]	49.1	99.2	140.4	226.1	-	-	-	-
SPN [48]	23.8	44.2	131.2	219.3	236.3	428.4	87.9	126.3
SPN+L2SM [48]	21.2	38.7	126.8	203.9	227.2	405.2	73.4	119.4
ScSiNet	20.96	36.38	118.19	214.13	194.63	370.85	69.23	107.44

ferability can be attributed to ScSiNet’s scale-invariant property as well, as the network is robust against scale and density variations across different datasets.

4.4 Ablation Study

To further understand the effectiveness of the proposed ScSiNet and randomly integrated loss, we perform a detailed ablation study over the three datasets.

Effects of Inter/Intra-layer Aggregations and Optimal G value in SiT . In order to demonstrate the importance of both interlayer and intralayer scale fusion, we first evaluate two variants of our model: No Interlayer and No Intralayer. The variant with no interlayer fusion is achieved by removing dense connections, whereas that with no intralayer setting degenerates to the DenseNet-like model. Due to lack of group convolution, no intralayer setting introduces a larger number of parameters. The ablative results show that both interlayer and intralayer are contributive to the improvements of counting performance; see Table 3. As discussed in Sec. 3.2, the hyper parameter G used in intralayer scale pyramid balances computational overhead and scale diversity. Here, we evaluate ScSiNet with different G values in Table 3 as well. It can be observed that our method performs well across different G values and achieves the best performance when G=6, which corresponds to 1.4M total parameters. Higher G value results in a modest increase in MAE due to potential overfitting under high model complexity.

Table 3. The impacts of inter/intra-layer scale fusion and the number of groups (G) in SiT on ShanghaiTech Part A dataset.

	No Inter (G=6)	No Intra (G=1)	G=2	G=4	G=6	G=8
Parameters	11.0M	20.9M	11.7M	12.9M	14.1M	15.3 M
MAE	57.00	60.11	60.04	58.85	55.77	57.50
MSE	96.77	104.67	104.50	95.83	90.23	98.60

Effectiveness of Stochastic Scale Mixer. We analyse the effectiveness of stochastic scale mixer on ShanghaiTech Part_A, Part_B and UCF-QNRF datasets. We compare the performances of the ScSiNet with and without scale mixer attached. The details are listed in Table 4, which demonstrates that our proposed scale mixer indeed plays a crucial role in the counting accuracy thanks to its stronger capability of integrating features at varying scales. To better understand the importance of stochastic fusion, we also compare the effects of the scale aggregation under fixed $\alpha=1$ and stochastic α respectively. As it can be observed from Table 4, consistent improvements are obtained from the stochastic strategy. This may be explained by that the stochastic α alleviates the sensibility to huge scale changes, thereby overcoming potential overfitting. Representative

samples under both settings are displayed in Fig. 6, which shows that the scale mixer is able to suppress the noisy details effectively while preserving sufficient scale information, thus helping to generate improved density maps.

Table 4. The effectiveness of stochastic scale mixer on ShanghaiTech Part_A, Part_B, and UCF-QNRF datasets. The setting (under $\alpha=1$) is not tested on UCF-QNRF due to limited computational resource.

	w.o Scale Mixer		w. Scale Mixer			
	MAE	MSE	(fixed $\alpha=1$)		(stochastic α)	
	MAE	MSE	MAE	MSE	MAE	MSE
Part_A	61.05	100.27	57.60	93.12	55.77	90.23
Part_B	7.01	11.53	6.96	11.21	6.79	10.95
UCF-QNRF	91.12	170.80	-	-	89.69	178.46

Effects of Randomly Integrated Loss. To explore the effectiveness of the proposed randomly integrated loss, we evaluate this strategy on Part_A and UCF_CC.50. The use of the proposed loss enables the network to be robust to huge density shifts even under very small training set (MAE 69.2 \rightarrow 55.77 on Part_A and 229.53 \rightarrow 154.87 on UCF_CC.50). As a result, significant improvement is achieved when compared to the training using single images (batch size is 1). The batch size N is a hyperparameter in our loss, it controls the balance between the computational costs and estimation precision. We test the model trained with $N=8, 16, 32$, and finally N is fixed as 16 with both high accuracy and low GPU usage.

5 Conclusion

In this paper, we propose a Single-column Scale-invariant Network (ScSiNet) to address the issues of scale variation, density shift, and overfitting in crowd counting. We extract and integrate multi-scale features via the combination of coarse-grained interlayer dense connections and the novel intralayer scale-invariant transformation (SiT). Furthermore, a randomly integrated loss is presented to make full use of small training sets and enlarge density diversity, which enables ScSiNet to be robust against huge density shifts. Extensive experiments demonstrate that the proposed method consistently and significantly outperforms the state-of-the-art methods. The prominent transferability of ScSiNet on datasets with varied density distributions and the strong capability of ScSiNet in handling downsampled test images are also clearly illustrated.

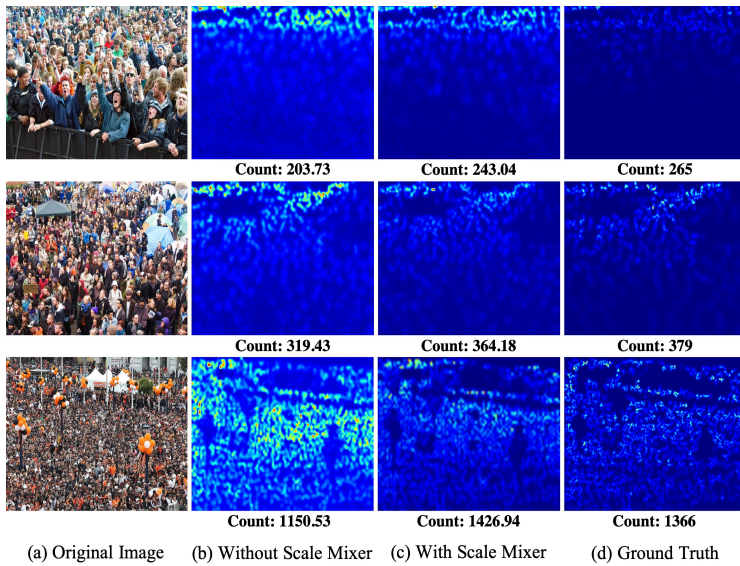


Fig. 6. Qualitative evaluation of the effectiveness of stochastic scale mixer. The three representative samples are from the ShanghaiTech Part A dataset and have varied densities.

References

1. Cai, Z., Fan, Q., Feris, R.S., Vasconcelos, N.: A unified multi-scale deep convolutional neural network for fast object detection. In: european conference on computer vision. pp. 354–370. Springer (2016)
2. Cao, X., Wang, Z., Zhao, Y., Su, F.: Scale aggregation network for accurate and efficient crowd counting. In: Proceedings of the European Conference on Computer Vision (ECCV). pp. 734–750 (2018)
3. Chen, K., Gong, S., Xiang, T., Change Loy, C.: Cumulative attribute space for age and crowd density estimation. In: Proceedings of the IEEE conference on computer vision and pattern recognition. pp. 2467–2474 (2013)
4. Chen, K., Loy, C.C., Gong, S., Xiang, T.: Feature mining for localised crowd counting. In: BMVC. vol. 1, p. 3 (2012)
5. Chen, L.C., Yang, Y., Wang, J., Xu, W., Yuille, A.L.: Attention to scale: Scale-aware semantic image segmentation. In: Proceedings of the IEEE conference on computer vision and pattern recognition. pp. 3640–3649 (2016)
6. Cheng, Z.Q., Li, J.X., Dai, Q., Wu, X., Hauptmann, A.: Learning spatial awareness to improve crowd counting. arXiv preprint arXiv:1909.07057 (2019)
7. Chollet, F.: Xception: Deep learning with depthwise separable convolutions. In: Proceedings of the IEEE conference on computer vision and pattern recognition. pp. 1251–1258 (2017)
8. Dalal, N., Triggs, B.: Histograms of oriented gradients for human detection (2005)
9. Deb, D., Ventura, J.: An aggregated multicolumn dilated convolution network for perspective-free counting. In: Proceedings of the IEEE Conference on Computer Vision and Pattern Recognition Workshops. pp. 195–204 (2018)
10. Dollar, P., Wojek, C., Schiele, B., Perona, P.: Pedestrian detection: An evaluation of the state of the art. *IEEE transactions on pattern analysis and machine intelligence* **34**(4), 743–761 (2011)
11. Gastaldi, X.: Shake-shake regularization. arXiv preprint arXiv:1705.07485 (2017)
12. Ge, W., Collins, R.T.: Marked point processes for crowd counting. In: 2009 IEEE Conference on Computer Vision and Pattern Recognition. pp. 2913–2920. IEEE (2009)
13. Guerrero-Gómez-Olmedo, R., Torre-Jiménez, B., López-Sastre, R., Maldonado-Bascón, S., Onoro-Rubio, D.: Extremely overlapping vehicle counting. In: Iberian Conference on Pattern Recognition and Image Analysis. pp. 423–431. Springer (2015)
14. Guo, D., Li, K., Zha, Z.J., Wang, M.: Dadnet: Dilated-attention-deformable convnet for crowd counting. In: Proceedings of the 27th ACM International Conference on Multimedia. pp. 1823–1832. ACM (2019)
15. He, K., Zhang, X., Ren, S., Sun, J.: Deep residual learning for image recognition. In: Proceedings of the IEEE conference on computer vision and pattern recognition. pp. 770–778 (2016)
16. Hsieh, M.R., Lin, Y.L., Hsu, W.H.: Drone-based object counting by spatially regularized regional proposal network. In: Proceedings of the IEEE International Conference on Computer Vision. pp. 4145–4153 (2017)
17. Huang, G., Liu, Z., Van Der Maaten, L., Weinberger, K.Q.: Densely connected convolutional networks. In: Proceedings of the IEEE conference on computer vision and pattern recognition. pp. 4700–4708 (2017)
18. Idrees, H., Saleemi, I., Seibert, C., Shah, M.: Multi-source multi-scale counting in extremely dense crowd images. In: Proceedings of the IEEE conference on computer vision and pattern recognition. pp. 2547–2554 (2013)

19. Idrees, H., Tayyab, M., Athrey, K., Zhang, D., Al-Maadeed, S., Rajpoot, N., Shah, M.: Composition loss for counting, density map estimation and localization in dense crowds. In: Proceedings of the European Conference on Computer Vision (ECCV). pp. 532–546 (2018)
20. Jiang, X., Xiao, Z., Zhang, B., Zhen, X., Cao, X., Doermann, D., Shao, L.: Crowd counting and density estimation by trellis encoder-decoder networks. In: Proceedings of the IEEE Conference on Computer Vision and Pattern Recognition. pp. 6133–6142 (2019)
21. Lempitsky, V., Zisserman, A.: Learning to count objects in images. In: Advances in neural information processing systems. pp. 1324–1332 (2010)
22. Li, W., Mahadevan, V., Vasconcelos, N.: Anomaly detection and localization in crowded scenes. *IEEE transactions on pattern analysis and machine intelligence* **36**(1), 18–32 (2013)
23. Li, Y., Zhang, X., Chen, D.: Csrnet: Dilated convolutional neural networks for understanding the highly congested scenes. In: Proceedings of the IEEE conference on computer vision and pattern recognition. pp. 1091–1100 (2018)
24. Lin, T.Y., Dollar, P., Girshick, R., He, K., Hariharan, B., Belongie, S.: Feature pyramid networks for object detection. In: The IEEE Conference on Computer Vision and Pattern Recognition (CVPR) (July 2017)
25. Liu, L., Qiu, Z., Li, G., Liu, S., Ouyang, W., Lin, L.: Crowd counting with deep structured scale integration network. Proceedings of the IEEE International Conference on Computer Vision (2019)
26. Liu, N., Long, Y., Zou, C., Niu, Q., Pan, L., Wu, H.: Adcrowdnet: An attention-injective deformable convolutional network for crowd understanding. In: Proceedings of the IEEE Conference on Computer Vision and Pattern Recognition. pp. 3225–3234 (2019)
27. Liu, W., Salzmann, M., Fua, P.: Context-aware crowd counting. In: Proceedings of the IEEE Conference on Computer Vision and Pattern Recognition. pp. 5099–5108 (2019)
28. Liu, X., van de Weijer, J., Bagdanov, A.D.: Leveraging unlabeled data for crowd counting by learning to rank. In: Proceedings of the IEEE Conference on Computer Vision and Pattern Recognition. pp. 7661–7669 (2018)
29. Lowe, D.G.: Distinctive image features from scale-invariant keypoints. *International journal of computer vision* **60**(2), 91–110 (2004)
30. Ma, Z., Wei, X., Hong, X., Gong, Y.: Bayesian loss for crowd count estimation with point supervision. *ICCV* (2019)
31. Najibi, M., Samangouei, P., Chellappa, R., Davis, L.S.: Ssh: Single stage headless face detector. In: Proceedings of the IEEE International Conference on Computer Vision. pp. 4875–4884 (2017)
32. Onoro-Rubio, D., López-Sastre, R.J.: Towards perspective-free object counting with deep learning. In: European Conference on Computer Vision. pp. 615–629. Springer (2016)
33. Paszke, A., Gross, S., Chintala, S., Chanan, G., Yang, E., DeVito, Z., Lin, Z., Desmaison, A., Antiga, L., Lerer, A.: Automatic differentiation in pytorch (2017)
34. Ranjan, V., Le, H., Hoai, M.: Iterative crowd counting. In: Proceedings of the European Conference on Computer Vision (ECCV). pp. 270–285 (2018)
35. Roy, A., Todorovic, S.: A multi-scale cnn for affordance segmentation in rgb images. In: European conference on computer vision. pp. 186–201. Springer (2016)
36. Sam, D.B., Surya, S., Babu, R.V.: Switching convolutional neural network for crowd counting. In: 2017 IEEE Conference on Computer Vision and Pattern Recognition (CVPR). pp. 4031–4039. IEEE (2017)

37. Shen, Z., Xu, Y., Ni, B., Wang, M., Hu, J., Yang, X.: Crowd counting via adversarial cross-scale consistency pursuit. In: Proceedings of the IEEE conference on computer vision and pattern recognition. pp. 5245–5254 (2018)
38. Shi, M., Yang, Z., Xu, C., Chen, Q.: Revisiting perspective information for efficient crowd counting. In: Proceedings of the IEEE Conference on Computer Vision and Pattern Recognition. pp. 7279–7288 (2019)
39. Shi, Z., Mettes, P., Snoek, C.G.M.: Counting with focus for free (2019)
40. Shi, Z., Zhang, L., Liu, Y., Cao, X., Ye, Y., Cheng, M.M., Zheng, G.: Crowd counting with deep negative correlation learning. In: Proceedings of the IEEE conference on computer vision and pattern recognition. pp. 5382–5390 (2018)
41. Simonyan, K., Zisserman, A.: Very deep convolutional networks for large-scale image recognition. arXiv preprint arXiv:1409.1556 (2014)
42. Sindagi, V.A., Patel, V.M.: Generating high-quality crowd density maps using contextual pyramid cnns. In: Proceedings of the IEEE International Conference on Computer Vision. pp. 1861–1870 (2017)
43. Sindagi, V.A., Patel, V.M.: Multi-level bottom-top and top-bottom feature fusion for crowd counting. Proceedings of the IEEE International Conference on Computer Vision (2019)
44. Viola, P., Jones, M.J., Snow, D.: Detecting pedestrians using patterns of motion and appearance. *International Journal of Computer Vision* **63**(2), 153–161 (2005)
45. Wu, Y., He, K.: Group normalization. In: Proceedings of the European Conference on Computer Vision (ECCV). pp. 3–19 (2018)
46. Xie, S., Girshick, R., Dollár, P., Tu, Z., He, K.: Aggregated residual transformations for deep neural networks. In: Proceedings of the IEEE conference on computer vision and pattern recognition. pp. 1492–1500 (2017)
47. Xiong, H., Lu, H., Liu, C., Liu, L., Cao, Z., Shen, C.: From open set to closed set: Counting objects by spatial divide-and-conquer (2019)
48. Xu, C., Qiu, K., Fu, J., Bai, S., Xu, Y., Bai, X.: Learn to scale: Generating multi-polar normalized density map for crowd counting. Proceedings of the IEEE International Conference on Computer Vision (2019)
49. Yan, Z., Yuan, Y., Zuo, W., Tan, X., Wang, Y., Wen, S., Ding, E.: Perspective-guided convolution networks for crowd counting (2019)
50. Zhang, A., Yue, L., Shen, J., Zhu, F., Zhen, X., Cao, X., Shao, L.: Attentional neural fields for crowd counting. In: ICCV (2019)
51. Zhang, H., Cisse, M., Dauphin, Y.N., Lopez-Paz, D.: mixup: Beyond empirical risk minimization. arXiv preprint arXiv:1710.09412 (2017)
52. Zhang, S., Wu, G., Costeira, J.P., Moura, J.M.: Fcn-rlstm: Deep spatio-temporal neural networks for vehicle counting in city cameras. In: Proceedings of the IEEE International Conference on Computer Vision. pp. 3667–3676 (2017)
53. Zhang, S., Wu, G., Costeira, J.P., Moura, J.M.: Understanding traffic density from large-scale web camera data. In: Proceedings of the IEEE Conference on Computer Vision and Pattern Recognition. pp. 5898–5907 (2017)
54. Zhang, X., Zhou, X., Lin, M., Sun, J.: Shufflenet: An extremely efficient convolutional neural network for mobile devices. In: Proceedings of the IEEE Conference on Computer Vision and Pattern Recognition. pp. 6848–6856 (2018)
55. Zhang, Y., Zhou, D., Chen, S., Gao, S., Ma, Y.: Single-image crowd counting via multi-column convolutional neural network. In: Proceedings of the IEEE conference on computer vision and pattern recognition. pp. 589–597 (2016)
56. Zhao, H., Shi, J., Qi, X., Wang, X., Jia, J.: Pyramid scene parsing network. In: Proceedings of the IEEE conference on computer vision and pattern recognition. pp. 2881–2890 (2017)